Spatiotemporal transformations of ultrashort terahertz pulses

Petr Kužel, Maxim A. Khazan, and Jan Kroupa

Institute of Physics, Academy of Sciences of the Czech Republic, Na Slovance 2, 182 21 Prague 8, Czech Republic

Received March 12, 1999; revised manuscript received June 14, 1999

We have experimentally studied the propagation in free space and through focusing optics of subpicosecond half- and single-cycle terahertz pulses emitted by large-aperture emitters. The spatial transformations of the beams are connected to phase changes and effective frequency filtering and lead to spectacular changes in the pulse time profile. The experimental results are in excellent agreement with the predictions of a simple analytical model based on a Gaussian-beam approximation. © 1999 Optical Society of America [S0740-3224(99)01210-2]

OCIS codes: 320.7120, 260.3090, 350.5500.

1. INTRODUCTION

Starting from the mid-1980s, a variety of materials were reported to emit subpicosecond terahertz (THz) pulses. Two rather distinct mechanisms have been used for the generation of such pulses: optical rectification in crystals with large second-order nonlinearities, such as $LiTaO_3$ (Ref. 1) or DAST (Ref. 2), and photoconductive switches integrated in dipole antenna structures that use current surges to radiate into free space.[3,4,5] More recently, THz radiation from both biased[6,7] and unbiased semiconductor surfaces in bulk semiconductor wafers[8] as well as from strained layer heterostructures[9] has been observed. Both photoconductive[10,11] and electro-optic sampling[12–16] detection techniques allow a phase-sensitive determination of the electric field waveform of the THz pulses. This makes it possible to use the described technique as a time-domain spectroscopic method[17–19] for investigation of polar excitations in the millimeter and submillimeter spectral range. This spectral range in fact constitutes a bridge between the classical IR spectroscopy domain and the frequencies accessible by microwave techniques.

THz radiation has to be transformed by far-infrared optics to be focused on the detection sensor and eventually on the smaller-size sample. Consequently, it is worth knowing in detail how the temporal waveform and the spectrum of the pulses are altered as a result of these spatial transformations.

THz beam transformations were described in the frame of Gaussian-beam optics first by Ziolkowski and Judkins,[20] who predicted the temporal reshaping of half-cycle pulses owing to free-space propagation; Kaplan[21] has recently extended this analytical calculation to pulses with arbitrary temporal profiles. Jepsen *et al.*[22] used the *ABCD* matrix formalism to simulate the propagation of a THz beam; You and Bucksbaum[23] used this formalism to calculate numerically the changes of time profile and spectra of the pulses that are due to the transformations by a lens or a mirror. Feng *et al.*[24] elucidated the role of the phase shift near the focal plane in the reshaping of the pulse. A numerical model based on the scalar diffraction theory has also been reported (Ref. 25). This last study was focused on the near-field phenomena: A comparison of the model with the measurements in the near field was presented.

In this paper we report a detailed systematic experimental study demonstrating the spatiotemporal transformations of ultrashort THz pulses in the far and the near fields, and we quantitatively compare the results with the theoretical predictions. We show that the results are in a very good agreement with a simple analytical model based on the Gaussian-beam transformations in the spectral domain. The presented model is developed for large-aperture emitters, and the calculations are restricted to the on-axis field; on the other hand, analytical results are obtained that allow very simple modeling of complex experimental setups.

2. THEORETICAL DESCRIPTION

The theoretical description has the same basis as that presented by You and Bucksbaum.[23] We consider a diffraction-limited THz beam generated by a large-aperture (typically several millimeters) photoconductive emitter, and we transform it by using the Gaussian-beam propagation formalism.[26]

By $E(t)$, $e(\nu)$ we denote the Fourier pair of the THz electric field waveform:

$$e(\nu) = \int_{-\infty}^{\infty} E(t)\exp(-2\pi i \nu t)\,\mathrm{d}t. \tag{1}$$

We are interested only in the on-axis field shape; consequently, within the Gaussian-beam approximation, we can write[27]

$$e(\nu; z) = e_0(\nu)\,\frac{w_0}{w(z)}\exp\left\{-i\left[kz - \arctan\left(\frac{z}{z_0}\right)\right]\right\}, \tag{2}$$

where

$$w^2(z) = {w_0}^2\left[1 + \left(\frac{z}{z_0}\right)^2\right], \qquad z_0 = \frac{\pi {w_0}^2}{c}\nu; \tag{3}$$

w_0 stands for the beam-waist size; $e_0(\nu)$ determines the near-field waveform of the pulse and depends on the optical pump-beam profile and the physical properties of the emitter. We assume that the waist of the THz beam for all the transmitted frequencies is located on the emitter area: This is a reasonable assumption for the usual case in which the pump optical beam is not extremely convergent or divergent. We additionally assume that w_0 is equal to one-half of the gap between the emitter's electrodes for all wavelengths. The propagator term $\exp(-ikz)$ can be omitted in nondispersive media.

When the THz pulse propagates through any focusing optics, its spatial properties are modified following the *ABCD* matrix transformations.[26] However, for a long-wavelength and broadband radiation, as the studied THz beam is, it is necessary to take into account the lens aperture (denoted A). In our simple model we introduce the aperture in the following way: (i) if the beam size at the lens is smaller than its aperture, i.e., $w(L;\nu) < A/2$, then we assume that the beam is not affected by the finite lens size; (ii) if the beam size at the lens is larger than its aperture, i.e., $w(L;\nu) > A/2$, then the transformed beam size close to the lens is set to $w'(-L';\nu) = A/2$ [L' is the distance between the lens and the focal plane of the transformed beam; see Eq. (4)]. It is evident that such a cutoff resulting from the aperture leads to an effective long-wavelength filtering. The applicability of this treatment is tested by our experiments.

The beam parameters after the transformation and the cutoff take the form

$$L' = \frac{f(L^2 + {z_0}^2)(L^2 + {z_0}^2 - fL)}{(L^2 + {z_0}^2 - fL)^2 + f^2 {z_0}^2 X^2},$$

$$w_0' = w_0\left(\frac{L'f}{L^2 + {z_0}^2 - fL}\right)^{1/2} X,$$

$$z_0' = \frac{\pi w_0'^2}{c}\nu, \qquad w'^2(z) = w_0'^2\left[1 + \left(\frac{z}{z_0'}\right)^2\right] \tag{4}$$

with

$$\nu > \nu_m : X = 1, \tag{5a}$$

$$\nu < \nu_m : X = \left(\frac{2w_0}{A}\right)^2\left(\frac{L^2}{{z_0}^2} + 1\right), \tag{5b}$$

$$\nu_m = \alpha(L)[(2w_0/A)^2 - 1]^{1/2}, \tag{5c}$$

$$\alpha(z) = \frac{c}{\pi {w_0}^2} z = \frac{z}{z_0}\nu. \tag{5d}$$

Equations (4) with $X = 1$ can be greatly simplified in the domain of the beam optics validity, i.e., when the conditions $L, |L - f|, f \gg z_0$ are satisfied. Similar simplifications can be obtained even for $X \neq 1$ if an additional condition is satisfied. It can be expressed as

$$\left|\frac{fL}{L - f}\right| \ll \frac{\pi(A/2)^2}{\lambda} \tag{6}$$

and rejects the spectral components with the longest wavelengths. If all the above conditions are fulfilled, expressions (4) are reduced to very simple relations:

$$\nu_m = \alpha(L)\frac{2w_0}{A}, \qquad L' = \frac{fL}{L - f}$$

$$\nu > \nu_m : w_0' = w_0\frac{L'}{L},$$

$$\nu < \nu_m : w_0' = w_0\frac{L'}{L}\frac{\nu_m}{\nu}. \tag{7}$$

Let us return to the general case. The changes in the spectrum that are due to the transformation can be expressed as

$$e(\nu; z) = e_0(\nu)\frac{w_0}{w'(z)}\frac{w'(-L')}{w(L)} \times \exp\left\{ i\left[\arctan\left(\frac{L}{z_0}\right) - \arctan\left(\frac{-L'}{z_0'}\right) + \arctan\left(\frac{z}{z_0'}\right)\right]\right\}, \tag{8}$$

where z stands for the distance between the detection sensor and the transformed beam-waist position. The term $w'(-L')/w(L)$ accounts for the continuity of the on-axis amplitude after the beam has passed through the lens aperture. Taking into account definitions (3) of w and z_0, and analogous expressions for w' and z_0' [Eqs. (4)], Eq. (8) can be expressed in the very convenient form (a reflection on a mirror is described by the same expression multiplied by -1)

$$e(\nu; z) = e_0(\nu)\left[1 - i\frac{\alpha(L)}{\nu}\right]^{-1} \times \left[1 + i\frac{\alpha'(L')}{\nu}\right]\left[1 - i\frac{\alpha'(z)}{\nu}\right]^{-1}, \tag{9}$$

where $\alpha'(z) = cz/(\pi w_0'^2)$. The first term in the square brackets on the right-hand side is simply due to the free-space propagation before the lens. In the far-field limit this term provides

$$E(t) = \frac{1}{2\pi\alpha}\frac{\partial E_0(t)}{\partial t}; \tag{10}$$

i.e., the amplitude of the far field is indirectly proportional to z (through α), and the time-profile shape is a derivative of the near-field waveform, as expected.

The remaining two terms of Eq. (9) describe the transformation that is due to the lens and subsequent propagation in free space, respectively. It follows that any additional optics can be accounted for by multiplication of the right-hand side of Eq. (9) by a couple of analogous terms. This expression can be easily used for computer simulations of complicated optical paths.

One can easily study a particular case that is often applicable for the main part of the transmitted spectrum: It is the case in which the approximate formulas (7) can be applied to the beam transformations; i.e., the beam optics approximation is valid for all the spectral components. [In fact condition (6) is never satisfied for the longest wavelengths, but these spectral components are always efficiently filtered out as a result of the diffraction

and the aperture effect; their intensity is thus significantly lowered by the propagation process itself, and they cannot influence the results considerably.] Then the waist position does not depend on the wavelength.

We introduce the following notation (see Fig. 1): $e^{(n)}(\nu; z)$ is the field between the nth and the $(n+1)$th lenses, $e^{(n)}(\nu; 0)$ is its value in the waist position, and $\alpha_n(z)$ depends on the beam-waist size $w_{0,n}$ through Eq. (5d); D_n is the distance between the nth and the $(n+1)$th lenses, and L_n is the distance between the nth lens and the preceding beam waist: L_n and L_n' are related through Eq. (4).

One then obtains, for the electric field in the far field (near the lenses) and in the waist,

$$e^{(n-1)}(\nu; L_n) = e^{(n-1)}(\nu; 0)\frac{i\nu}{\alpha_{n-1}(L_n)}, \tag{11a}$$

$$e^{(n)}(\nu; 0) = e^{(n-1)}(\nu; L_n)\frac{iF_n(\nu)}{\nu}\alpha_{n-1}(L_n), \tag{11b}$$

$$e^{(n)}(\nu; 0) = -e^{(n-1)}(\nu; 0)F_n(\nu). \tag{11c}$$

The numerical factor $\alpha_{n-1}(L_n)$ describes the field changes that are due to focusing–defocusing. $F_n(\nu)$ is the amplitude spectral filter related to the aperture of the nth lens; it is given by the relations

$$\nu > \nu_m : F_n(\nu) = \frac{L_n}{L_n'}, \tag{12a}$$

$$\nu < \nu_m : F_n(\nu) = \frac{L_n}{L_n'}\left(\frac{\nu}{\nu_m}\right)^2. \tag{12b}$$

The filter's profile is a direct consequence of the manner of the lens aperture's introduction into the calculation. In particular, this filter has a discontinuous derivative at $\nu = \nu_m$, and therefore it provides an artificial oscillation in the time domain. The field in the time domain is in fact given by

$$E^{(n)}(t) = -\frac{L_n}{L_n'}E^{(n-1)}(t) * \left\{\delta(t) + 4\nu_m\left[\frac{\cos(\omega_m t)}{(\omega_m t)^2} - \frac{\sin(\omega_m t)}{(\omega_m t)^3}\right]\right\}, \tag{13}$$

where $\omega_m = 2\pi\nu_m$. The singularity in the filter frequency profile can be removed by a different profile choice (for instance, a Gaussian-like filter); thus the oscillations corresponding to $\sin x/x$ types of functions can be avoided. However, essential characteristics of the filter—its quadratic behavior in the low-frequency limit and frequency independence in the high-frequency limit—have to be preserved. A more detailed study of expression (13) shows that the main features of the pulse shape in the beam waist are similar (as the quadratic low-frequency filtering suggests) to the second derivative of the near field (at the emitter), i.e., to the first derivative of the far field (near the lens); practically, the filter effectively broadens the far-field waveform and adds one half-cycle to it.

If one chooses the far-field spectrum as a reference that provides the main characteristics of a particular emitter, then, as Eq. (11b) suggests, the spectral bandwidth in the beam waists will be narrower: It is a result of an effective linear low-frequency filtering and a $1/\nu$ high-frequency filtering. The final picture of the transformations through a set of lenses within the current approximation is depicted in Fig. 1. The pulse characteristics are related here to the far-field spectrum. The phase shift is always incremented by $\pi/2$ between the waist and the far field, and effective low- and high-frequency filters occur in the beam waists.

3. EXPERIMENTAL RESULTS AND DISCUSSION

Our experimental setup uses a Lexel 480 Ti:sapphire laser oscillator as the light source. The laser output has the following characteristics: pulse length of 80 fs, central wavelength of 800 nm, repetition rate of 76 MHz, and average power of 400 mW.

THz pulses were generated by a large-aperture photoconducting antenna made of semi-insulating GaAs:Cr that has a large free-carrier lifetime and provides very short half-cycle THz pulses; some experiments were also performed with a subpicosecond free-carrier lifetime sample of low-temperature–grown (LT) GaAs, providing single-cycle pulses. The emitters were endowed with golden electrodes with two different spacings (3 and 6 mm). The average photocurrent between the emitter electrodes was very high in GaAs:Cr (typically 1 mA for 800 V and 3-mm electrode spacing) owing to the large

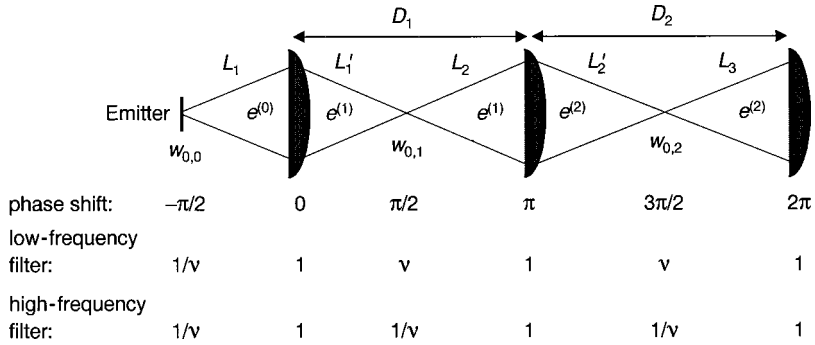

Fig. 1. Scheme of phase shifts and effective amplitude filters that result from propagation of the THz pulse through a set of lenses. Both filters and phase shifts refer to the far-field spectrum.

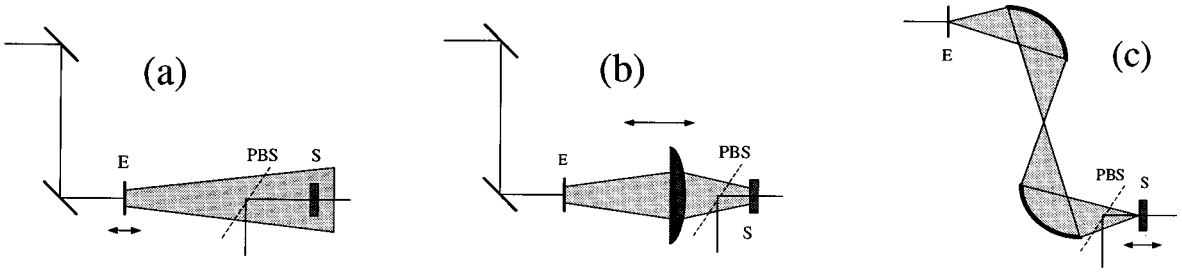

Fig. 2. Schematic of the experimental setups. (a) Free-space propagation measurement (emitter–sensor distance variable); (b) focusing with a sooted polyethylene lens (lens position variable); (c) focusing with a pair of ellipsoidal mirrors with one common focus (second mirror—sensor distance variable). *E*, emitter; *S*, sensor; PBS, pellicle beam splitter.

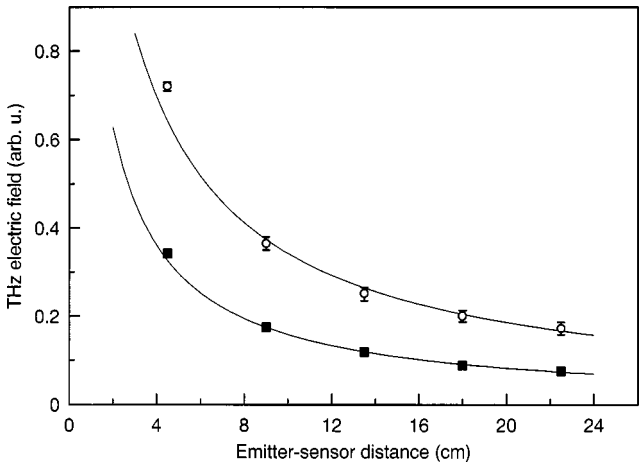

Fig. 3. Peak values of the waveforms (solid symbols) and integrated amplitude spectrum values (open symbols) as a function of the emitter–sensor distance in the setup of Fig. 2(a). Solid curves, fits with $\sim 1/l_{e-s}$ function.

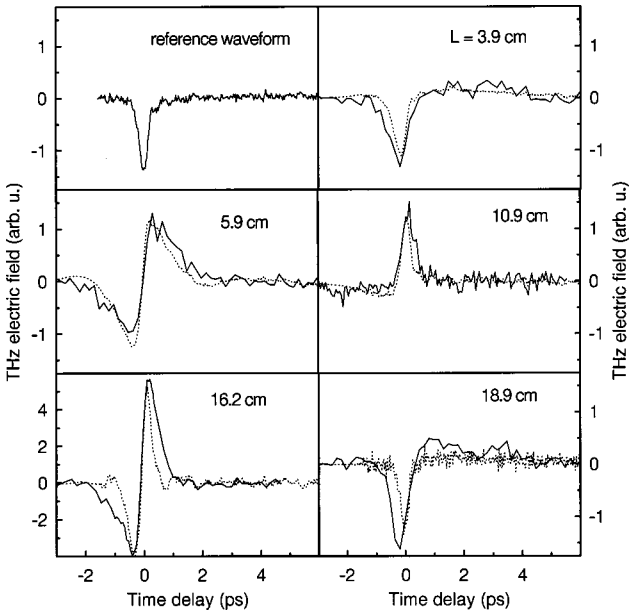

Fig. 4. Solid curves, waveforms taken by use of the setup in Fig. 2(b) (the emitter–lens distance is indicated in the figures). Dotted lines, simulations based on the numerical Fourier transform of formula (9); a reference waveform taken during the free-space propagation measurement alignment was introduced into the calculation to simulate $e_0(\nu)$. See the text for details.

free-carrier lifetime of the emitter; therefore the emitter was cooled by a cold air flow.

An electro-optic sampling technique similar to the one described in Ref. 28 with a 0.5-mm-thick ⟨110⟩ ZnTe sensor crystal was employed for time-resolved detection of the pulses. The bandwidth related to the sampling resolution was higher than the width of the emission spectrum.

In the first series of experiments the free-space propagation of the THz pulses without any focusing optics was studied [see Fig. 2(a)]. GaAs:Cr delivered half-cycle pulses with durations shorter than 400 fs. In the frequency domain the nonzero spectral density extended up to 2.5 or 3 THz. We measured the waveforms for several emitter—sensor distances l_{e-s} (from 4.5 to as long as 22.5 cm). These displacements resulted neither in pulse-shape changes nor in pulse spectral profile distortions. Figure 3 shows the dependence of the peak value of the waveform and of the integrated spectral amplitude of the signal on l_{e-s} for an emitter with a 3-mm electrode spacing. Both curves fit very well to $1/l$ dependence, indicating that, following Eq. (10), the far-field radiation is measured. This is in agreement with the theory that predicts that the frequency component of 1 THz reaches the far-field approximation at the distance of ~3 cm from the emitter.

In the second series of experiments [Fig. 2(b)] the GaAs:Cr emitter with a 3-mm electrode spacing was used, l_{e-s} distance was fixed at 22.5 cm, and a sooted polyethylene plano–convex lens (f = 4.3 cm) with one spherical surface was put between the emitter and the sensor. Waveforms were taken for various positions of the lens. During these experiments the spherical surface of the lens was directed toward the sensor, and the distances (emitter–lens l_{e-l} and lens–sensor l_{l-s}) were carefully evaluated: The positions of the principal points of the lens were taken into account. One set of measurements is shown in Fig. 4. The first waveform, denoted "reference," was taken without the lens for l_{e-s} = 7 cm, and it was used for the determination of $e_0(\nu)$ in the theoretical simulations. It was introduced through the numerical Fourier transform into Eq. (9), and the waveforms expected for various l_{e-l} were then calculated and compared with the profiles measured experimentally. Several points should be emphasized. (i) The amplitude and the time delay of the reference pulse were adjusted to correspond [after the transformation through Eq. (9)] to the amplitude and the time delay of the experimental wave-

form taken for $l_{e-l} = 3.9$ cm. (ii) No further modifications of the amplitude and delay were made for other studied emitter–lens distances. (iii) The distances l_{e-l} of 5.8 and 16.3 cm correspond to the situation when the sensor is placed exactly in the waist position of the transformed beam. For l_{e-l} greater than 5.8 cm and smaller than 16.3 cm the pulse passes through the waist before entering the sensor: This is why the polarity of the signal is opposite that of the reference pulse. (iv) Evidently the measured pulse shape and even its intensity correspond quite well to the predictions. Note, however, that the width of the waveforms obtained experimentally is slightly large compared with the predictions. We attribute this phenomenon to the spherical aberration of the lens. The broadening of waveforms is more pronounced when the lens is close to the sensor (l_{e-l} of 16.3 and 18.9 cm), i.e., when the spherical surface of the lens is close to the focus, as expected in the spherical aberration theory.

Finally, in the third series of experiments [Fig. 2(c)] a pair of aluminum ellipsoidal mirrors with equal effective focal lengths ($f = 7.5$ cm for 45° incidence) was introduced into the THz beam path so that the emitter was placed at one focus of the first mirror, one focus was common for both mirrors (a place for introducing a small sample in spectroscopic applications), and the sensor was positioned near the other focus of the second mirror.

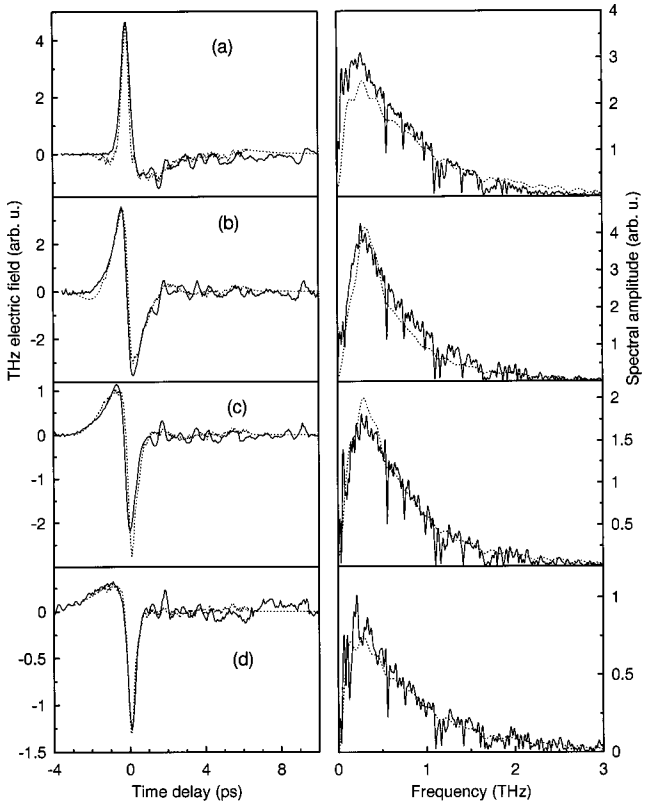

Fig. 5. THz waveforms and corresponding spectra obtained with a 3-mm GaAs:Cr emitter in the setup with two ellipsoidal mirrors for four different l_{m-s}. Dotted lines, simulations obtained from the reference waveform (same as in Fig. 4) based on Eq. (9) for two mirrors. l_{m-s} in centimeters: (a) experimental 11.5, model 13.5; (b) experimental 15, model 15; (c) experimental 19, model 16.5; and (d) experimental 26, model 20.

Then the mirror–sensor distance l_{m-s} was scanned. The experimental results and the results of simulations for the GaAs:Cr emitter with 3-mm electrode spacing are presented in Fig. 5. The sharp absorption lines in the measured spectra correspond to the water vapor rotational transitions.[19,29] The theoretical curves were calculated starting from the same reference waveform as for the lens experiments, and again the amplitude and time delay of the reference waveform were fixed for all the simulations. The agreement with the experiment is excellent for $l_{m-s} = 15$ cm [sensor exactly in the focus of the second mirror; Fig. 5(b)]. We can also get a very good agreement between the experiment and theory for the other positions of the sensor [see Fig. 5(a), 5(c), and 5(d)], but the distance l_{m-s} introduced into the model should differ systematically from the experimental one.

We repeated the set of experiments by using a larger GaAs:Cr emitter (6 mm). The detected bandwidth is narrower in this case, and the spectral amplitude peaks at half the frequency of the 3-mm emitter because the limit frequency ν_m is decreased by a factor of 2 in the setup with the larger emitter [see Eq. (7)]. Very good agreement of the theory and the experiment is achieved for the same distance mismatch as in the case of 3-mm emitter. We verified that within our model there is no parameter that, when varied around its experimental value, could compensate for the distance mismatch. On the other hand, we did not find any distance mismatch for the spherical lens case. It thus seems that the problem is probably related to the ellipticity of the mirrors.

In fact, our experiment suggests that the beam remains in a state close to its waist state for a longer distance than a Gaussian beam does and that at even longer distances it diverges faster (to fit the mirror aperture). The ellipticity of the mirrors introduces a radial distribution of the radius of curvature—the effective radius of curvature near the edge of the mirrors is smaller than in the center—and the spherical wavefront of the Gaussian beam is transformed by the reflection to a more complicated one:

$$\frac{1}{R_2(r)} = \frac{1}{R_1} - \frac{1}{f(r)}.$$

We tentatively attribute the observed effect to these distortions of the wavefront; however, to give a more quantitative answer, the scalar diffraction theory should be used, or experiments with toroidal instead of ellipsoidal mirrors should be performed.

On the other hand, the ellipsoidal mirrors should not introduce any spherical aberration: Indeed, no broadening of the experimental waveforms (similar to that discussed for the experiments with the spherical lens) was observed.

We also verified that the theoretical description provides correct results for bipolar type of the electric field time profile delivered by LT GaAs. Figure 6 shows a waveform obtained with a 3-mm emitter of LT GaAs in the far field (7 cm from the emitter) serving as a reference and a waveform transformed through two ellipsoidal mirrors. The agreement with the model is also very good.

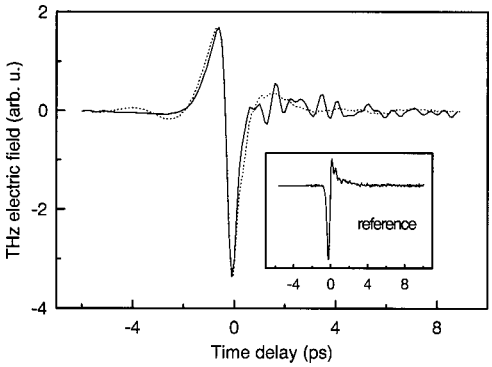

Fig. 6. THz waveforms and corresponding spectra obtained with 3-mm LT GaAs emitter. (a) Free-space propagation geometry [Fig. 2(a)], $l_{e-s} = 7$ cm; (b) setup with two ellipsoidal mirrors, $l_{m-s} = 15$ cm [Fig. 2(c)]. Dotted curves, simulations obtained from the reference waveform (a).

4. CONCLUSION

We present a systematic experimental study of the spatiotemporal transformations of ultrashort THz pulses during propagation along various optical paths including a far-infrared lens and ellipsoidal mirrors. We have shown that the model based on the Gaussian approximation of the beam propagation and transformation quantitatively can well account for the observed changes both in the time profile and in the spectra. In particular, the model emphasizes the role of the phase change during propagation and shows that the aperture of the optical elements acts as an effective spectral filter: Linear filtering occurs at low frequencies, and $1/\nu$ filtering occurs at high frequencies. These results allow better understanding of the shape of THz pulses detected with different techniques and can make an important contribution to the study of various emitters' characteristics and for THz time-domain spectroscopic applications.

ACKNOWLEDGMENTS

The authors are thankful to J. Oswald, D. Nohavica, L. Pekárek, W. Hansen, and I. Wilke for providing semiconductor emitter wafers. This work was supported by grants 202/96/0447 and 202/98/P022 of the Grant Agency of the Czech Republic.

REFERENCES

1. M. van Exter and D. R. Grischkowsky, "Characterization of an optoelectronic terahertz beam system," IEEE Trans. Microwave Theory Tech. **38**, 1684–1691 (1990).
2. D. H. Auston and M. C. Nuss, "Electro-optical generation and detection of femtosecond electrical transients," IEEE J. Quantum Electron. **24**, 184–197 (1988).
3. X.-C. Zhang, X. F. Ma, Y. Jin, T.-M. Lu, E. P. Boden, D. P. Phelps, K. R. Stewart, and C. P. Yakymyshyn, "Terahertz optical rectification from a nonlinear organic crystal," Appl. Phys. Lett. **61**, 3080–3082 (1992).
4. P. R. Smith, D. H. Auston, and M. C. Nuss, "Subpicosecond photoconducting dipole antennas," IEEE J. Quantum Electron. **24**, 255–260 (1988).
5. C. H. Fattinger and D. Grischkowsky, "Terahertz beams," Appl. Phys. Lett. **54**, 490–492 (1989).
6. B. B. Hu, J. T. Darrow, X.-C. Zhang, D. H. Auston, and P. R. Smith, "Optically steerable photoconducting antennas," Appl. Phys. Lett. **56**, 886–888 (1990).
7. J. T. Darrow, B. B. Hu, X.-C. Zhang, and D. H. Auston, "Subpicosecond electromagnetic pulses from large-aperture photoconducting antennas," Opt. Lett. **15**, 323–325 (1990).
8. X.-C. Zhang, B. B. Hu, J. T. Darrow, and D. H. Auston, "Generation of femtosecond electromagnetic pulses from semiconductor surfaces," Appl. Phys. Lett. **56**, 1011–1013 (1990).
9. X.-C. Zhang, B. B. Hu, S. H. Xin, and D. H. Auston, "Optically induced femtosecond electromagnetic pulses from GaSb/AlSb strained-layer superlattices," Appl. Phys. Lett. **57**, 753–755 (1990).
10. Ch. Fattinger and D. Grischkowsky, "Point source terahertz optics," Appl. Phys. Lett. **53**, 1480–1482 (1988).
11. D. H. Auston, K. P. Cheung, and P. R. Smith, "Picosecond photoconducting Hertzian dipoles," Appl. Phys. Lett. **45**, 284–286 (1984).
12. D. H. Auston, K. P. Cheung, J. A. Valdmanis, and D. A. Kleinman, "Cherenkov radiation from femtosecond optical pulses in electro-optic media," Phys. Rev. Lett. **53**, 1555–1558 (1984).
13. Q. Wu and X.-C. Zhang, "Free-space electro-optic sampling of terahertz beams," Appl. Phys. Lett. **67**, 3523–3525 (1995).
14. Q. Wu, M. Litz, and X.-C. Zhang, "Broadband detection capability of ZnTe electro-optic field detectors," Appl. Phys. Lett. **68**, 2924–2926 (1996).
15. P. U. Jepsen, C. Winnewisser, M. Schall, V. Schyja, S. R. Keiding, and H. Helm, "Detection of THz pulses by phase retardation in lithium tantalate," Phys. Rev. E **53**, R3052–R3054 (1996).
16. A. Nahata, D. H. Auston, T. F. Heinz, and C. J. Wu, "Coherent detection of freely propagating terahertz radiation by electro-optic sampling," Appl. Phys. Lett. **68**, 150–152 (1996).
17. D. Grischkowsky, S. Keiding, M. van Exter, and Ch. Fattinger, "Far-infrared time-domain spectroscopy with terahertz beams of dielectrics and semiconductors," J. Opt. Soc. Am. B **7**, 2006–2015 (1990).
18. D. H. Auston and K. P. Cheung, "Coherent time-domain far-infrared spectroscopy," J. Opt. Soc. Am. B **2**, 606–612 (1985).
19. M. van Exter, Ch. Fattinger, and D. Grishkowsky, "Terahertz time-domain spectroscopy of water vapor," Opt. Lett. **14**, 1128–1130 (1989).
20. R. W. Ziolkowski and J. B. Judkins, "Propagation characteristics of ultrawide-bandwidth pulsed Gaussian beams," J. Opt. Soc. Am. A **9**, 2021–2030 (1992).
21. A. E. Kaplan, "Diffraction-induced transformation of near-cycle and subcycle pulses," J. Opt. Soc. Am. B **15**, 951–956 (1998).
22. P. U. Jepsen, R. H. Jacobsen, and S. R. Keiding, "Generation and detection of terahertz pulses from biased semiconductor antennas," J. Opt. Soc. Am. B **13**, 2424–2436 (1996).
23. D. You and P. H. Bucksbaum, "Propagation of half-cycle far infrared pulses," J. Opt. Soc. Am. B **14**, 1651–1655 (1997).
24. S. Feng, H. G. Winful, and R. W. Hellwarth, "Gouy shift and temporal reshaping of focused single-cycle electromagnetic pulses," Opt. Lett. **23**, 385–387 (1998).
25. E. Budiarto, N.-W. Pu, S. Jeong, and J. Bokor, "Near-field propagation of terahertz pulses from a large-aperture antenna," Opt. Lett. **23**, 213–215 (1998).
26. H. Kogelnik, "On the propagation of Gaussian beams of light through lenslike media including those with a loss or gain variation," Appl. Opt. **4**, 1562–1569 (1965).
27. A. Yariv and P. Yeh, *Optical Waves in Crystals* (Wiley, New York, 1984), Chap. 2.
28. Q. Wu and X.-C. Zhang, "Ultrafast electro-optic field sensors," Appl. Phys. Lett. **68**, 1604–1606 (1996).
29. G. W. Chantry, "Spectroscopy at optical and longer wavelengths," in *Long-Wave Optics* (Academic, London, 1984), Vol. 2, p. 456.